

Inductive-detection electron-spin resonance spectroscopy with 65 spins/ $\sqrt{\text{Hz}}$ sensitivity

S. Probst, A. Bienfait, P. Campagne-Ibarcq, J. J. Pla, B. Albanese, J. F. Da Silva Barbosa, T. Schenkel, D. Vion, D. Esteve, K. Mølmer, J. J. L. Morton, R. Heeres, and P. Bertet

Citation: *Appl. Phys. Lett.* **111**, 202604 (2017);

View online: <https://doi.org/10.1063/1.5002540>

View Table of Contents: <http://aip.scitation.org/toc/apl/111/20>

Published by the [American Institute of Physics](#)

Articles you may be interested in

[Sensitive spin detection using an on-chip SQUID-waveguide resonator](#)

Applied Physics Letters **111**, 202601 (2017); 10.1063/1.5006693

[Realization of zero-field skyrmions with high-density via electromagnetic manipulation in Pt/Co/Ta multilayers](#)

Applied Physics Letters **111**, 202403 (2017); 10.1063/1.5001322

[High-kinetic inductance additive manufactured superconducting microwave cavity](#)

Applied Physics Letters **111**, 202602 (2017); 10.1063/1.5000241

[On-chip nanofluidic integration of acoustic sensors towards high Q in liquid](#)

Applied Physics Letters **111**, 203501 (2017); 10.1063/1.4992046

[Oxygen-assisted synthesis of hexagonal boron nitride films for graphene transistors](#)

Applied Physics Letters **111**, 203103 (2017); 10.1063/1.5001790

[Eliminating the non-Gaussian spectral response of X-ray absorbers for transition-edge sensors](#)

Applied Physics Letters **111**, 192602 (2017); 10.1063/1.5001198

Scilight

Sharp, quick summaries **illuminating**
the latest physics research

Sign up for **FREE!**



Inductive-detection electron-spin resonance spectroscopy with 65 spins/ $\sqrt{\text{Hz}}$ sensitivity

S. Probst,¹ A. Bienfait,^{1,2} P. Campagne-Ibarcq,^{1,3} J. J. Pla,⁴ B. Albanese,¹ J. F. Da Silva Barbosa,¹ T. Schenkel,⁵ D. Vion,¹ D. Esteve,¹ K. Mølmer,⁶ J. J. L. Morton,⁷ R. Heeres,¹ and P. Bertet^{1,a)}

¹Quantronics Group, SPEC, CEA, CNRS, Université Paris-Saclay, CEA Saclay, 91191 Gif-sur-Yvette Cedex, France

²Institute for Molecular Engineering, University of Chicago, Chicago, Illinois 60637, USA

³Departments of Applied Physics and Physics, Yale University, New Haven, Connecticut 06520, USA

⁴School of Electrical Engineering and Telecommunications, University of New South Wales, Anzac Parade, Sydney, NSW 2052, Australia

⁵Accelerator Technology and Applied Physics Division, Lawrence Berkeley National Laboratory, Berkeley, California 94720, USA

⁶Department of Physics and Astronomy, Aarhus University, Ny Munkegade 120, DK-8000 Aarhus C, Denmark

⁷London Centre for Nanotechnology, University College London, London WC1H 0AH, United Kingdom

(Received 30 August 2017; accepted 10 October 2017; published online 14 November 2017)

We report electron spin resonance spectroscopy measurements performed at millikelvin temperatures in a custom-built spectrometer comprising a superconducting micro-resonator at 7 GHz and a Josephson parametric amplifier. Owing to the small ($\sim 10^{-12} \lambda^3$) magnetic resonator mode volume and to the low noise of the parametric amplifier, the spectrometer's single shot sensitivity reaches 260 ± 40 spins/echo translating into 65 ± 10 spins/ $\sqrt{\text{Hz}}$ for repeated acquisition. Published by AIP Publishing. <https://doi.org/10.1063/1.5002540>

Electron spin resonance (ESR) is a well-established spectroscopic method to analyze paramagnetic species, utilized in materials science, chemistry, and molecular biology to characterize reaction products and complex molecules.¹ In a conventional pulsed ESR spectrometer based on the so-called inductive detection method, the paramagnetic spins precess in an external magnetic field B_0 and radiate weak microwave signals into a resonant cavity, whose emissions are amplified and measured.

Despite its widespread use, ESR has limited sensitivity, and large amounts of spins are necessary to accumulate sufficient signal. Most conventional ESR spectrometers operate at room temperature and employ three-dimensional cavities. At X-band,² they require on the order of $\sim 10^{13}$ spins to obtain sufficient signal in a single echo.¹ Enhancing this sensitivity to smaller spin ensembles is a major research subject. This has been achieved by employing alternative detection schemes including optically detected magnetic resonance (ODMR),^{3,4} scanning probe based techniques,^{5–9} SQUIDS,¹⁰ and electrically detected magnetic resonance.^{11,12} For instance, ODMR achieves single spin sensitivity through optical readout of the spin state. However, this requires the presence of suitable optical transitions in the energy spectrum of the system of interest, which makes it less versatile.

In recent years, there has been a parallel effort to enhance the sensitivity of inductive ESR detection.^{13–20} This development has been triggered by the progress made in the field of circuit quantum electrodynamics (cQED),²¹ where high fidelity detection of weak microwave signals is essential for the measurement and manipulation of superconducting quantum circuits. In particular, it has been theoretically predicted²² that single-spin sensitivity should be reachable by combining high

quality factor superconducting micro-resonators and Josephson Parametric Amplifiers (JPAs),²³ which are sensitive microwave amplifiers adding as little noise as allowed by quantum mechanics to the incoming spin signal. Based on this principle, ESR spectroscopy measurements¹⁸ demonstrated a sensitivity of 1700 spins/ $\sqrt{\text{Hz}}$. In this work, we build on these efforts and show that, by optimizing the superconducting resonator design, the sensitivity can be enhanced to the level of 65 spins/ $\sqrt{\text{Hz}}$.

Figure 1(a) shows a schematic design of the spectrometer consisting of a superconducting LC resonant circuit capacitively coupled to the measurement line with energy decay rate κ_c and internal losses κ_i . The resonator is slightly over-coupled ($\kappa_c \geq \kappa_i$) and probed in reflection at its resonance frequency ω_r . This micro-resonator is inductively coupled to the spin ensemble and cooled to 12 mK in a dilution refrigerator. The signal leaking out of the resonator, which contains in particular the spin signal, is first amplified by a JPA operating in the degenerate mode,^{24,25} followed by a High-Electron-Mobility Transistor (HEMT) amplifier at 4 K and further amplifiers at room-temperature. The two signal quadratures $I(t)$ and $Q(t)$ are obtained by homodyne demodulation at ω_r . More details on the setup can be found in Ref. 18.

Compared to Ref. 18, the micro-resonator was redesigned with the goal of enhancing the spin-resonator coupling constant $g = \gamma_e \langle 0|S_x|1 \rangle \delta B_1$, where $\langle 0|S_x|1 \rangle \approx 0.5$ for the transition used in the following. Here, $\gamma_e/2\pi = 28$ GHz/T denotes the gyromagnetic ratio of the electron, $|0\rangle$ and $|1\rangle$ the ground and excited states of the spin, \mathbf{S} the electron spin operator, and δB_1 the magnetic field vacuum fluctuations. Reducing the inductor size to a narrow wire decreases the magnetic mode volume²⁶ and therefore enhances δB_1 . In the new design, shown in Fig. 1(b), most of the resonator consists of an interdigitated capacitor, shunted by an $l = 100 \mu\text{m}$

^{a)}patrice.bertet@cea.fr

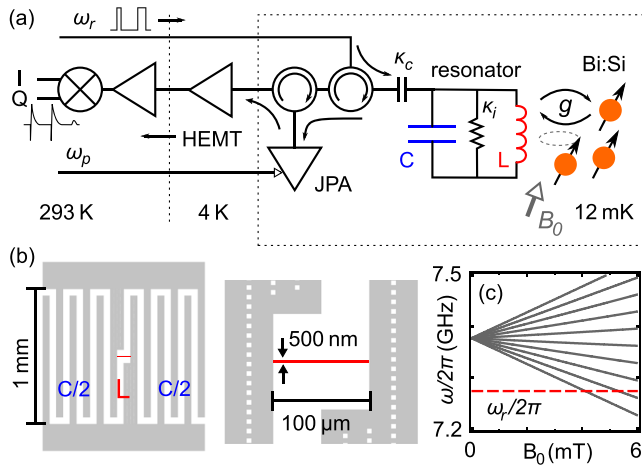


FIG. 1. (a) Schematic of the experiment: Bi:Si spins, biased by a dc magnetic field B_0 , are coupled to a LC resonator of frequency ω_r . Microwave control pulses at ω_p are sent to the resonator input. The reflected signal and the signals emitted by the spins are first amplified by a JPA operated in the degenerate mode followed by further amplification and homodyne demodulation to obtain the signal quadratures $I(t)$ and $Q(t)$. (b) Design of the planar lumped element LC resonator. (c) ESR-allowed transitions of the Bi donor spins vs. B_0 . The dashed line indicates the resonator frequency.

long, $w = 500$ nm wide, and $t = 100$ nm-thick wire inductance. It is patterned out of an aluminum thin-film by electron-beam lithography followed by lift-off, on top of an isotopically enriched ^{28}Si sample (purity: 99.95%) containing a peak concentration of $8 \times 10^{16} \text{ cm}^{-3}$ bismuth donors implanted at a depth of 100 ± 50 nm. The details of the implantation process are described in Refs. 18 and 27. Based on electromagnetic simulations,²⁸ an impedance of 32Ω and a magnetic mode volume of $\sim 10^{-12} \lambda^3$ (0.2 pico-liters) are estimated, resulting in a spin-resonator coupling of $g/2\pi \approx 4.3 \times 10^2$ Hz. Note that the magnetic field is concentrated along the $100 \mu\text{m}$ long central inductor wire such that only spins in this region couple efficiently to the resonator and contribute to the signal. The resonator properties are characterized at 12 mK by microwave reflection measurements,^{29,30} yielding $\omega_r/2\pi = 7.274$ GHz, $\kappa_c = 3.4 \times 10^5 \text{ s}^{-1}$, $\kappa_i = 2.5 \times 10^5 \text{ s}^{-1}$, and a total loss rate of $\kappa_l = \kappa_i + \kappa_c = 5.9 \pm 0.1 \times 10^5 \text{ s}^{-1}$, measured at a power corresponding to a single photon on average in the resonator.³¹ This translates into loaded (unloaded) quality factors of $Q_l = \omega_r/\kappa_l = 7.8 \times 10^4$ ($Q_i = \omega_r/\kappa_i = 1.8 \times 10^5$).

At low temperatures, bismuth donors in the silicon sample trap an additional valence electron to the surrounding host silicon atoms, which can be probed through electron spin resonance.^{32,33} The electron spin $S = 1/2$ experiences a strong hyperfine interaction ($A/2\pi = 1.45$ GHz) with the ^{209}Bi nuclear spin $I = 9/2$ giving rise to a zero field splitting of 7.38 GHz. The full Hamiltonian is given by $H/\hbar = \gamma_e \mathbf{S} \cdot \mathbf{B} - \gamma_n \mathbf{I} \cdot \mathbf{B} + A \mathbf{S} \cdot \mathbf{I}$, where $\gamma_n/2\pi = 7$ MHz/T denotes the gyromagnetic ratio of the nucleus. Note that the Bi spin system is also interesting in the context of quantum information processing because it features clock transitions where the coherence time can reach 2.7 s.³⁴ In addition, the large zero field splitting makes this system well suited for integration with superconducting circuits. Figure 1(c) shows the low field spectrum of the ESR-allowed transitions close

to the resonator frequency. The dashed line marks the spectrometer resonator frequency at $\omega_r/2\pi = 7.274$ GHz.

For the sensitivity of the spectrometer, two quantities are relevant: the minimum number of spins N_{min} necessary to produce a single echo with a signal-to-noise ratio (SNR) of 1 and the number of spins that can be measured with unit SNR within 1 s of integration time $N_{min}/\sqrt{N_{seq}}$, where N_{seq} is the number of experimental sequences per second. This time-scale is determined by the spin energy relaxation time T_1 , and we typically wait $T_{rep} \geq 3T_1$ between measurements. In our experiment, the lowest transition of the Bi ensemble is tuned into resonance with the cavity by applying $B_0 = 3.74$ mT parallel to the $100 \mu\text{m}$ long central inductor wire. In order to address all spins within the cavity bandwidth, we choose the duration t_p of our square pulses $0.5 \mu\text{s}$ for the $\pi/2$ and $1 \mu\text{s}$ for the π pulse such that $t_p \kappa_l \lesssim 1$. The π pulse amplitude was determined by recording Rabi oscillations on the echo signal, see Fig. 2(c). Figure 2(a) shows a full echo sequence (red circles). The reflected control pulses show a rapid rise followed by a slower decay due to the resonator ringdown, leading to an asymmetric echo shape.

In order to simulate the data, knowledge of g is necessary.¹⁸ It is experimentally obtained from spin relaxation data, as explained in the next paragraph, leaving no other adjustable parameter than the number of spins excited by the first $\pi/2$ pulse. The quantitative agreement, see the blue line in Fig. 2(a), allows us to state that $N_e = 234 \pm 35$ spins are contributing to the echo. N_e is defined through the polarization created by the first $\pi/2$ pulse. For details on the simulation, we refer to Ref. 18. The ESR signal is given by the echo area A_e , and in order to extract the SNR, a series of echo traces was recorded. Each echo trace is then integrated, weighted by its expected mode shape, which constitutes a matched filter maximizing the SNR.¹⁸ From the resulting histogram, shown in Fig. 2(b), we deduce a SNR of 0.9 per

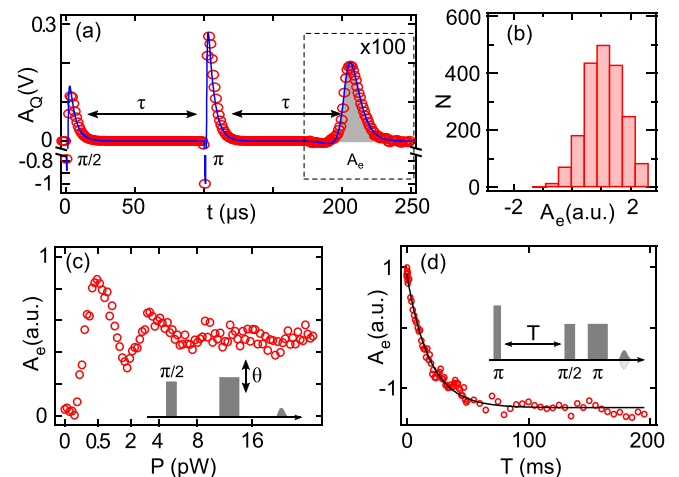


FIG. 2. (a) Measured (red circles) and simulated (blue line) quadrature signals showing the π and $\pi/2$ pulses as well as the echo. (b) Histogram of A_e . These data are obtained by subtracting two consecutive experimental traces with opposite $\pi/2$ pulse phases (phase cycling¹⁸) so that the single-echo SNR is obtained from the histogram width multiplied by $\sqrt{2}$. (c) Rabi oscillations of A_e , recorded by varying the power of the second pulse of the spin echo sequence. (d) Spin relaxation time measurement. A_e measured as a function of the delay T between an initial $1 \mu\text{s}$ -long π pulse and a subsequent spin-echo sequence (red open circles). An exponential fit (black solid line) yields $T_1 = 18.6$ ms.

single trace, yielding a single shot sensitivity of $N_{\min} = 260 \pm 40$ spins per echo. This result is consistent with an estimate of $N_{\min}^{(\text{th})} = \frac{\kappa_l}{2gp} \sqrt{\frac{mV}{\kappa_c}} \approx 10^2$ spins using the theory developed in Ref. 18. Here, $n=0.5$ is the number of noise photons, $p = 1 - \exp(-t/T_1) \approx 0.95$ the polarization, and $w \approx \kappa_l$ the effective inhomogeneous spin linewidth. Since the experiment was repeated at a rate of 16 Hz, this single echo sequence translates into an absolute sensitivity of 65 ± 10 spins/ $\sqrt{\text{Hz}}$. This figure may be increased further by irradiating the resonator with squeezed vacuum, as demonstrated in Ref. 19.

Figure 2(d) shows the longitudinal decay of the spin ensemble. It was obtained with an inversion recovery pulse sequence: first, a 1 μs -long π pulse inverts the spin ensemble followed by a spin echo detection sequence with 5 μs and 10 μs -long pulses after a variable time T . The exponential fit yields $T_1 = 18.6 \pm 0.5$ ms. Although the intrinsic spin lifetime of donors in silicon was measured to be 1.6×10^3 s,^{35,36} the coupling to the small-mode-volume and high-quality-factor resonator enhances significantly the spins' energy relaxation by spontaneous emission of microwave photons into the environment at rate $T_1^{-1} = 4g^2/\kappa_l$.³⁵ This allows us to experimentally determine that $g/2\pi = 450 \pm 11$ Hz, which is close to the value estimated from design. This Purcell limited spin relaxation also explains why we are exclusively sensing spins below the narrow wire. Spins located below the remaining part of the resonator have a ~ 100 fold reduced coupling (due to the $100\times$ larger width) giving rise to a 10^4 times longer T_1 , so that these spins are effectively unpolarized, and to 100 times smaller Rabi angles of the control pulses leading to unmeasurable echo amplitudes.

Figure 3(a) displays a Hahn-echo field sweep, i.e., A_e as a function of B_0 applied parallel to the inductor. The curve shows a large inhomogeneous broadening with Bi spins detected even at $B_0 = 0$ mT, which are thus shifted by approximately 100 MHz from the nominal zero-field value,

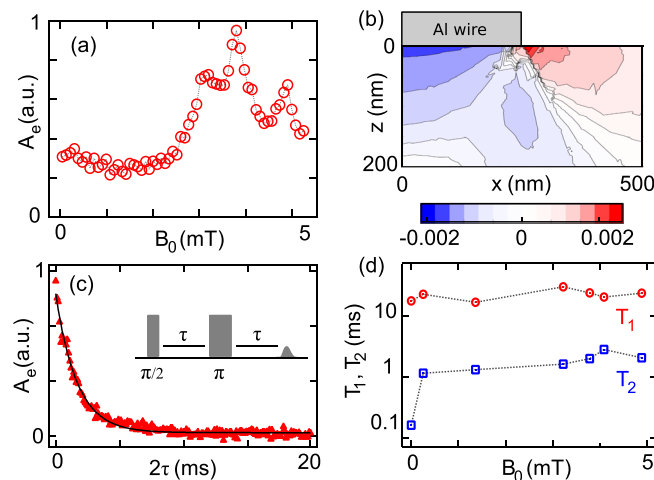


FIG. 3. (a) Echo-detected field sweep. A_e (open circles) is shown as a function of B_0 (parallel to the wire). (b) COMSOL simulation of the ϵ_{100} component of the strain field in the silicon around the wire. (c) Spin coherence time measurement at $B_0 = 3.74$ mT. A_e plotted as a function of the delay 2τ between $\pi/2$ pulse and echo (red triangles). An exponential fit (black solid line) yields $T_2 = 1.65 \pm 0.03$ ms. (d) T_1 and T_2 as a function of B_0 . Error bars are within the marker size.

see Fig. 1(c). We attribute this broadening to strain exerted by the aluminum resonator onto the Si substrate resulting from a difference in their coefficients of thermal expansion.^{18,37,38} Figure 3(b) displays a COMSOL[®] simulation of the ϵ_{100} component of the strain tensor. The impact of strain on the Bi spectrum is subject of active experimental and theoretical research.^{37,39} We have investigated the dependence of the spin coherence and relaxation times on B_0 , as shown in Fig. 3(d). A typical coherence time measurement, recorded at $B_0 = 3.74$ mT by measuring A_e as a function of 2τ , is shown in Fig. 3(c). The data are well fitted by an exponential decay with $T_2 = 1.65 \pm 0.03$ ms presumably limited by dipolar interactions with neighboring spins and charge noise. Note that the measured spectrometer sensitivity does not depend on T_2 , provided it is larger than the detection sequence duration. As expected, T_1 shows nearly no dependence on B_0 , because neither g nor κ_l varies significantly in the observed field range. In contrast, T_2 decreases weakly towards lower magnetic fields and drops abruptly at zero field. This behavior might originate from dipolar interactions with the residual ^{29}Si nuclear spin bath, which become relevant at low magnetic fields given the ^{29}Si concentration of 0.05%.

The sensitivity of the current spectrometer can be further enhanced by using multiple refocusing pulses to generate several echoes per sequence. Here, we employ the Carr-Purcell-Meiboom-Gill (CPMG) sequence,^{1,40} which consists of a $\pi/2$ pulse applied along the x-axis followed by n π pulses along the y-axis of the Bloch sphere. Assuming uncorrelated Gaussian noise, the increase of SNR is given by the CPMG echo decay curve $\text{SNR}(n)/\text{SNR}(1) = \frac{1}{\sqrt{n}} \sum_{i=1}^n A_e(t_i)$, where the index i labels the echoes from 1 to n along the sequence. The individual echoes during the first millisecond are presented in Fig. 4(a).

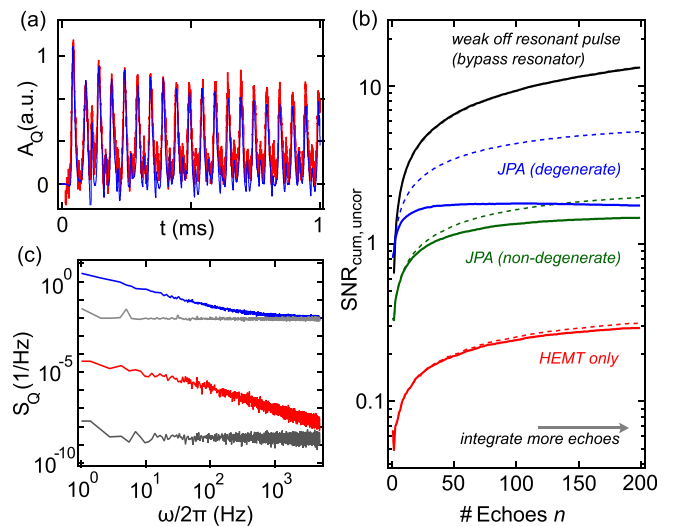


FIG. 4. (a) Averaged quadrature signal (red solid line) and simulation (blue solid line) showing the echoes recorded during the first millisecond of the CPMG sequence. (b) SNR vs. number of averaged CPMG echoes employing just the HEMT amplifier, the JPA in the non-degenerate mode, the JPA in the degenerate mode, and a control experiment, see text for details. Solid lines show the data and dashed lines the expected gain in SNR assuming uncorrelated noise. (c) Normalized quadrature noise power spectrum $S_Q(\omega)$ of the resonator at high (red) and low (blue) power corresponding to an average population of 10^6 and 3 photons in the cavity, respectively. Both bright and dark gray traces show the corresponding off-resonant noise traces for comparison.

The refocusing pulses are not visible in this plot because they are canceled by phase cycling. The blue line, computed by the simulation presented in Fig. 2(a) and using the same system parameters, is in good agreement with the data.

In order to quantify the gain in SNR, we record up to 4×10^4 single CPMG traces containing 200 echoes each. The data are then analyzed in two ways presented in Fig. 4(b) by dashed and solid lines, respectively: First, each echo in each sequence is integrated individually and its mean \bar{x}_i and standard deviation Δx_i are calculated in order to determine the $\text{SNR}_i = \bar{x}_i/\Delta x_i$ of the i -th echo. Provided that the noise is uncorrelated, the cumulative SNR sum over n echoes is given by $\text{SNR}_{\text{uncor}} = \frac{1}{\sqrt{n}} \sum_{i=1}^n \text{SNR}_i$. Second, we determine the actual cumulative $\text{SNR}_{\text{cum}} = \bar{x}_{\text{cum}}/\Delta x_{\text{cum}}$ by summing up all echoes in each trace up to the n -th echo and subsequently calculate the mean and standard deviation. Figure 4(b) shows the result for the spectrometer operating just with a HEMT amplifier, with the JPA in phase preserving mode and with the JPA in the degenerate mode. Without the JPA, $\text{SNR}_{\text{uncor}} \approx \text{SNR}_{\text{cum}}$ yielding a gain in SNR of up to 6. Employing the JPA, the gain initially follows the expectation for $\text{SNR}_{\text{uncor}}$ but then saturates. In particular, in the highest sensitivity mode, CPMG only allows for an increase in the SNR by approximately a factor of 2, thus reaching 33 spins/ $\sqrt{\text{Hz}}$. We interpret the discrepancy between SNR_{cum} and $\text{SNR}_{\text{uncor}}$ as a sign that correlations exist between the noise on the echoes of a given sequence, or in other words that low-frequency noise is present in our system.

To investigate whether this low-frequency noise is caused by the microwave setup (including the JPA), we perform a control experiment by replacing the echoes by weak coherent pulses of similar strength, which are reflected at the resonator input without undergoing any phase shift because they are purposely detuned by $\sim 25\kappa_l$ from ω_r . Figure 4(b) shows that $\text{SNR}_{\text{uncor}} = \text{SNR}_{\text{cum}}$ for this reference measurement (black dashed and solid lines are superimposed), indicating that the JPA itself is not responsible for the observed low-frequency noise. Instead, we attribute the sensitivity saturation in the echo signal to phase noise of our resonator. Figure 4(c) presents the normalized on and off resonance quadrature noise power spectra $S_Q(\omega)$ of the out-of-phase quadrature⁴¹ for two different powers. The noise originating from the resonator (blue and red lines) shows a $S_Q(\omega) \propto 1/\omega$ dependence dominating the background white noise (gray and black lines). For the low power measurement (blue line), corresponding to an average population of 3 photons in the resonator, we obtain a rms frequency noise of 7 kHz, which is 7% of $\kappa_l/2\pi$. This amount of phase noise is commonly observed in superconducting micro-resonators.⁴¹ Compared to low power, the high power spectrum (red line), corresponding to an average population of 10^6 photons, shows significantly less noise and we find that $S_Q(\omega)$ scales with the square-root of the intra-cavity power.^{31,41} This suggests that origin of the low-frequency excess noise lies in the presence of dielectric and/or paramagnetic defects.^{42–45} Note that off-resonant Bi spins would not show a power dependence and can therefore be excluded as a relevant noise source.

In conclusion, we have presented spin-echo measurements with a sensitivity of 65 spins/ $\sqrt{\text{Hz}}$, setting a new

state-of-the-art for inductively detected ESR. This was obtained by employing a low mode volume planar superconducting resonator in conjunction with a quantum limited detection chain. The energy lifetime of the spins was limited by the Purcell effect to 20 ms, allowing for fast repeating measurements. Due to the long coherence time of the spin system under investigation, Bi donors in ²⁸Si, it was possible to enhance the sensitivity further by a CPMG sequence to 33 spins/ $\sqrt{\text{Hz}}$. Achieving the maximum theoretical sensitivity with CPMG of 11 spins/ $\sqrt{\text{Hz}}$ was most likely hindered by the phase noise of the resonator. The sub pico-liter detection volume of our spectrometer makes it an interesting tool for investigating paramagnetic surfaces and, in particular, recently discovered 2D materials.^{46,47} This requires magnetic field resilient superconductors^{20,48} such as Nb, NbN, or NbTiN, which would also allow operation at higher temperatures.

We acknowledge technical support from P. Sénat and P.-F. Orfila, as well as stimulating discussions within the Quantronics Group. We acknowledge support of the European Research Council under the European Community's Seventh Framework Programme (FP7/2007-2013) through Grant Agreement Nos. 615767 (CIRQUSS), 279781 (ASCENT), and 630070 (quRAM) and of the ANR project QIPSE as well as the Villum Foundation.

¹A. Schweiger and G. Jeschke, *Principles of Pulse Electron Paramagnetic Resonance* (Oxford University Press, 2001).

²X-band frequency range: 8 to 12 GHz.

³J. Wrachtrup, C. Von Borczyskowski, J. Bernard, M. Orritt, and R. Brown, *Nature* **363**, 244 (1993).

⁴A. Gruber, A. Dräbenstedt, C. Tietz, L. Fleury, J. Wrachtrup, and C. v. Borczyskowski, *Science* **276**, 2012 (1997).

⁵S. Baumann, W. Paul, T. Choi, C. P. Lutz, A. Ardavan, and A. J. Heinrich, *Science* **350**, 417 (2015).

⁶Y. Manassen, R. J. Hamers, J. E. Demuth, and A. J. Castellano, Jr., *Phys. Rev. Lett.* **62**, 2531 (1989).

⁷D. Rugar, C. Yannoni, and J. Sidles, *Nature* **360**, 563 (1992).

⁸D. Rugar, R. Budakian, H. Mamin, and B. Chui, *Nature* **430**, 329 (2004).

⁹M. Grinolds, M. Warner, K. De Greve, Y. Dovzhenko, L. Thiel, R. Walsworth, S. Hong, P. Maletinsky, and A. Yacoby, *Nat. Nanotechnol.* **9**, 279 (2014).

¹⁰R. V. Chamberlin, L. A. Moberly, and O. G. Symko, *J. Low Temp. Phys.* **35**, 337 (1979).

¹¹F. Hoehne, L. Dreher, J. Behrends, M. Fehr, H. Huebl, K. Lips, A. Schegg, M. Suckert, M. Stutzmann, and M. S. Brandt, *Rev. Sci. Instrum.* **83**, 043907 (2012).

¹²A. Morello, J. J. Pla, F. A. Zwanenburg, K. W. Chan, K. Y. Tan, H. Huebl, M. Möttönen, C. D. Nugroho, C. Yang, J. A. van Donkelaar *et al.*, *Nature* **467**, 687 (2010).

¹³R. Narkowicz, D. Suter, and I. Niemeyer, *Rev. Sci. Instrum.* **79**, 084702 (2008).

¹⁴L. Shtirberg, Y. Twig, E. Dikarov, R. Halevy, M. Levit, and A. Blank, *Rev. Sci. Instrum.* **82**, 043708 (2011).

¹⁵Y. Kubo, I. Diniz, C. Grezes, T. Umeda, J. Isoya, H. Sumiya, T. Yamamoto, H. Abe, S. Onoda, T. Ohshima, V. Jacques, A. Dréau, J.-F. Roch, A. Auffeves, D. Vion, D. Esteve, and P. Bertet, *Phys. Rev. B* **86**, 064514 (2012).

¹⁶H. Malissa, D. I. Schuster, A. M. Tyryshkin, A. A. Houck, and S. A. Lyon, *Rev. Sci. Instrum.* **84**, 025116 (2013).

¹⁷A. J. Sigillito, H. Malissa, A. M. Tyryshkin, H. Riemann, N. V. Abrosimov, P. Becker, H.-J. Pohl, M. L. W. Thewalt, K. M. Itoh, J. J. L. Morton, A. A. Houck, D. I. Schuster, and S. A. Lyon, *Appl. Phys. Lett.* **104**, 222407 (2014).

¹⁸A. Bienfait, J. Pla, Y. Kubo, M. Stern, X. Zhou, C.-C. Lo, C. Weis, T. Schenkel, M. Thewalt, D. Vion, D. Esteve, B. Julsgaard, K. Moelmer, J. Morton, and P. Bertet, *Nat. Nanotechnol.* **11**, 253 (2015).

- ¹⁹A. Bienfait, P. Campagne-Ibarcq, A. Holm-Küilerich, X. Zhou, S. Probst, J. J. Pla, T. Schenkel, D. Vion, D. Esteve, J. J. L. Morton, K. Moelmer, and P. Bertet, *Phys. Rev. X* **7**, 041011 (2017).
- ²⁰C. Eichler, A. J. Sigillito, S. A. Lyon, and J. R. Petta, *Phys. Rev. Lett.* **118**, 037701 (2017).
- ²¹M. H. Devoret and R. J. Schoelkopf, *Science* **339**, 1169 (2013).
- ²²P. Haikka, Y. Kubo, A. Bienfait, P. Bertet, and K. Mølmer, *Phys. Rev. A* **95**, 022306 (2017).
- ²³X. Zhou, V. Schmitt, P. Bertet, D. Vion, W. Wustmann, V. Shumeiko, and D. Esteve, *Phys. Rev. B* **89**, 214517 (2014).
- ²⁴C. M. Caves, *Phys. Rev. D* **26**, 1817 (1982).
- ²⁵T. Yamamoto, K. Inomata, M. Watanabe, K. Matsuba, T. Miyazaki, W. D. Oliver, Y. Nakamura, and J. S. Tsai, *Appl. Phys. Lett.* **93**, 042510 (2008).
- ²⁶S. Haroche and J.-M. Raimond, *Exploring the Quantum* (Oxford University Press, 2006).
- ²⁷C. D. Weis, C. C. Lo, V. Lang, A. M. Tyryshkin, R. E. George, K. M. Yu, J. Bokor, S. A. Lyon, J. J. L. Morton, and T. Schenkel, *Appl. Phys. Lett.* **100**, 172104 (2012).
- ²⁸CST Microwave Studio[®], COMSOL Multiphysics[®].
- ²⁹D. M. Pozar, *Microwave Engineering*, 4th ed. (Wiley, 2011).
- ³⁰S. Probst, F. B. Song, P. A. Bushev, A. V. Ustinov, and M. Weides, *Rev. Sci. Instrum.* **86**, 024706 (2015).
- ³¹A. D. O'Connell, M. Ansmann, R. C. Bialczak, M. Hofheinz, N. Katz, E. Lucero, C. McKenney, M. Neeley, H. Wang, E. M. Weig, A. N. Cleland, and J. M. Martinis, *Appl. Phys. Lett.* **92**, 112903 (2008).
- ³²G. Feher, *Phys. Rev.* **114**, 1219 (1959).
- ³³G. W. Morley, M. Warner, A. M. Stoneham, P. T. Greenland, J. van Tol, C. W. Kay, and G. Aeppli, *Nat. Mater.* **9**, 725 (2010).
- ³⁴G. Wolfowicz, A. M. Tyryshkin, R. E. George, H. Riemann, N. V. Abrosimov, P. Becker, H.-J. Pohl, M. L. W. Thewalt, S. A. Lyon, and J. J. L. Morton, *Nat. Nanotechnol.* **8**, 561 (2013).
- ³⁵A. Bienfait, J. Pla, Y. Kubo, X. Zhou, M. Stern, C.-C. Lo, C. Weis, T. Schenkel, D. Vion, D. Esteve, J. Morton, and P. Bertet, *Nature* **531**, 74 (2016).
- ³⁶A. M. Tyryshkin, S. Tojo, J. J. L. Morton, H. Riemann, N. V. Abrosimov, P. Becker, H.-J. Pohl, T. Schenkel, M. L. W. Thewalt, K. M. Itoh, and S. A. Lyon, *Nat. Mater.* **11**, 143 (2012).
- ³⁷J. J. Pla, A. Bienfait, G. Pica, J. Mansir, F. A. Mohiyaddin, A. Morello, T. Schenkel, B. W. Lovett, J. J. L. Morton, and P. Bertet, e-print [arXiv:1608.07346](https://arxiv.org/abs/1608.07346).
- ³⁸T. Thorbeck and N. M. Zimmerman, *AIP Adv.* **5**, 087107 (2015).
- ³⁹J. Mansir, P. Conti, Z. Zeng, J. J. Pla, P. Bertet, B. Sklenard, Y.-M. Niquet, and J. J. L. Morton, e-print [arXiv:1710.00723](https://arxiv.org/abs/1710.00723).
- ⁴⁰F. Mentink-Vigier, A. Collauto, A. Feintuch, I. Kaminker, V. Tarle, and D. Goldfarb, *J. Magn. Reson.* **236**, 117 (2013).
- ⁴¹J. Gao, J. Zmuidzinas, B. A. Mazin, H. G. LeDuc, and P. K. Day, *Appl. Phys. Lett.* **90**, 102507 (2007).
- ⁴²S. E. de Graaf, A. A. Adamyan, T. Lindström, D. Erts, S. E. Kubatkin, A. Y. Tzalenchuk, and A. V. Danilov, *Phys. Rev. Lett.* **118**, 057703 (2017).
- ⁴³C. Wang, C. Axline, Y. Y. Gao, T. Brecht, Y. Chu, L. Frunzio, M. H. Devoret, and R. J. Schoelkopf, *Appl. Phys. Lett.* **107**, 162601 (2015).
- ⁴⁴J. Gao, M. Daal, A. Vayonakis, S. Kumar, J. Zmuidzinas, B. Sadoulet, B. A. Mazin, P. K. Day, and H. G. LeDuc, *Appl. Phys. Lett.* **92**, 152505 (2008).
- ⁴⁵S. Sendelbach, D. Hover, A. Kittel, M. Mück, J. M. Martinis, and R. McDermott, *Phys. Rev. Lett.* **100**, 227006 (2008).
- ⁴⁶A. K. Geim and I. V. Grigorieva, *Nature* **499**, 419 (2013).
- ⁴⁷K. S. Novoselov, A. Mishchenko, A. Carvalho, and A. H. Castro Neto, *Science* **353**, aac9439 (2016).
- ⁴⁸S. E. de Graaf, A. V. Danilov, A. Adamyan, T. Bauch, and S. E. Kubatkin, *J. Appl. Phys.* **112**, 123905 (2012).